Title

Structure of a human rhinovirus-bivalently bound antibody complex: implications for viral neutralization and antibody flexibility.

Journal

Proceedings of the National Academy of Sciences of the United States of America, 90(15)

ISSN

0027-8424

Authors

Smith, TJ
Olson, NH
Cheng, RH
et al.

Publication Date

1993-08-01

DOI

10.1073/pnas.90.15.7015

Peer reviewed

Proc. Natl. Acad. Sci. USA
Vol. 90, pp. 7015–7018, August 1993
Immunology

Structure of a human rhinovirus–bivalently bound antibody complex: Implications for viral neutralization and antibody flexibility

THOMAS J. SMITH*, NORMAN H. OLSON, R. HOLLAND CHENG, ELAINE S. CHASE, AND TIMOTHY S. BAKER

Department of Biological Sciences, Purdue University, West Lafayette, IN 47907

Communicated by Michael G. Rossmann, April 23, 1993

ABSTRACT **The structure of a neutralizing immunoglobulin (monoclonal antibody mAb17-IA), bound to human rhinovirus 14 (HRV14), has been determined by cryo-electron microscopy and image reconstruction. The antibody bound bivalently across icosahedral twofold axes of the virus, and there were no detectable conformational changes in the capsid. Thus, bivalently bound IgGs do not appear to cause gross deformations in the capsid. Differences between the electron density of the constant domains of the bound Fab fragment and IgG structures suggested that conformational changes occur about elbow axes upon bivalent attachment as was previously predicted. No significant density was observed for the Fc fragment, which adds further evidence for a high degree of mobility about the hinge region.**

Picornaviruses form one of the largest animal virus families (1) and include such members as rhinovirus, poliovirus, Coxsackie virus, foot-and-mouth disease virus, and hepatitis A virus. These small viruses are ≈30% RNA by weight and have a relative mass of $\approx 8.5 \times 10^6$ daltons. Their external, icosahedral shell is ≈300 Å in diameter and is composed of 60 copies of four viral coat proteins: VP1, VP2, VP3, and VP4. The structures of several of these viruses have been solved to atomic resolution (for a review, see ref. 2) including human rhinovirus 14 (HRV14) (3).

The study of spontaneous mutations in the viral coat that permitted the virus to escape antibody-mediated neutralization led to the identification of neutralizing immunogenic (NIm) sites on the surface of HRV14 (4, 5). These mutations clustered into four groups: NIm-IA, NIm-IB, NIm-II, and NIm-III (3). The monoclonal antibody (mAb) used in this study, mAb17-IA [isotype IgG2a (6)], binds to the NIm-IA site at the loop between the B and C strands of the VP1 β-barrel. This antigenic site is defined by natural escape mutations at Asp-91 and Glu-95 of VP1.

The mechanisms of antibody-mediated neutralization of picornaviruses are not well understood. Antibodies have been postulated to neutralize infectivity by inducing structural changes in the capsid (7, 8), by interfering with attachment (9), or possibly by preventing uncoating by intracapsid cross-linking (10). The latter hypothesis suggested that strongly neutralizing antibodies such as mAb17-IA might bind bivalently across icosahedral twofold axes. This proposal was firmly supported by the Fab fragment–virus complex (Fab17-IA–HRV14) structure (6), which was examined at ≈28-Å resolution with cryo-electron microscopy and image reconstruction techniques, and showed that Fab17-IA molecules bound in orientations that favored bivalent attachment of the immunoglobulin. It was further speculated that such bivalent binding might be facilitated by rotations of the Fab domains about the elbow axes. This study did not reveal any evidence for gross conformational changes in the capsid but could not rule out the possibility of such changes occurring if the intact antibody were to bind bivalently.

A number of electron microscopy studies of intact immunoglobulins bound to large antigens have illustrated the range of flexibility within antibodies (e.g., refs. 11 and 12). However, none of these studies examined intact antibodies bound bivalently to an antigenic surface, nor did they examine the relative rotations of the Fab variable ($V_L \cdot V_H$) and constant ($C_L \cdot C_H1$) heavy (H) and light (L) chain domains with respect to the elbow axes.

METHODS

mAb17-IA hybridomas were obtained from Roland Rueckert's laboratory at the University of Wisconsin. The hybridomas were grown in a Cellmax Quad-4 microcapillary system (Cellco, Germantown, MD), and the antibody was purified from the cellular supernatant on a protein G affinity column as described (6). Purity and integrity of the mAb17-IA was checked with reducing and nonreducing SDS/PAGE analysis. IgG–HRV14 complex was formed by mixing virus with a large excess of antibody with an ultrasonic homogenizer and high-salt buffers. Approximately 1 mg of virus (in ≈5–10 ml of buffer) was added to ≈30 ml of a solution of mAb17-IA at 1–2 mg/ml (the antibody-to-virus molar ratio was >1000) in 50 mM Tris buffer, pH 7.5/0.3 M NaCl. The virus was added slowly to the antibody solution and sonicated at maximum power with a microtip-equipped homogenizer. The high-salt concentration and ultrasonic homogenizer were necessary because the antibody was not very soluble. The resulting mixture was then incubated overnight at 4°C and concentrated to ≈8 ml (total volume) with Centricon-10 microconcentrators (Amicon). At no time did the solution become opalescent or did precipitate form. The mixture was then applied to a size-exclusion chromatography column (Superose 6; Pharmacia LKB) equilibrated with 50 mM Tris, pH 7.5/0.3 M NaCl. This gel matrix separated the IgG–virus complex and virus alone from the unbound antibody. The peaks representing IgG–HRV14 complex were then collected and used immediately for cryo-electron microscopy studies.

Cryo-electron microscopy was performed essentially as described (6, 13). Micrographs were recorded at ×49,000 magnification, ≈1.0 μm underfocus, and under minimal dose conditions on a Philips EM420 electron microscope (Philips Electronic Instruments, Mahwah, NJ) equipped with a Gatan 626 cryotransfer holder (Gatan, Warrendale, PA). We used 40 and 35 virion images to calculate the reconstructions for the Fab and IgG complexes, respectively, using established procedures (6). The effective resolutions of the reconstructions were 27 Å and 28 Å for the Fab and IgG complexes,

The publication costs of this article were defrayed in part by page charge payment. This article must therefore be hereby marked "*advertisement*" in accordance with 18 U.S.C. §1734 solely to indicate this fact.

Abbreviations: HRV14, human rhinovirus 14; mAb, monoclonal antibody; NIm sites, neutralizing immunogenic sites.

*To whom reprint requests should be addressed.

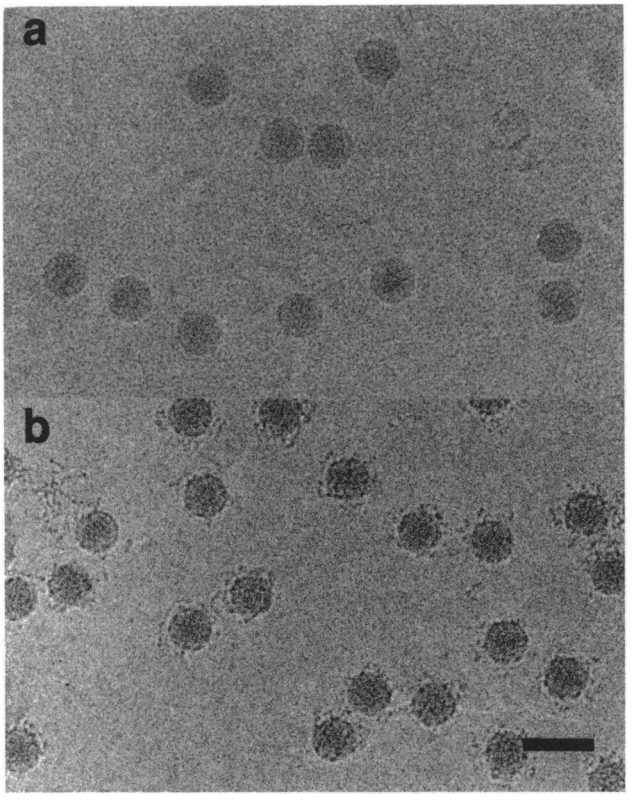

FIG. 1. Cryo-electron micrographs of native HRV14 (*a*) and of the HRV14–IgG complex (*b*). (Bar = 500 Å.)

respectively. The calculated eigenvalues of each data set exceed 10.0, which indicated that random and unique data were used for each reconstruction (14). The intensities of the electron density maps were scaled and then Fourier-transformed. The resulting set of structure factors for each complex were corrected for effects of the contrast transfer function and then back-transformed as described (6, 15).

RESULTS AND DISCUSSION

The IgG–virus (mAb17-1A–HRV14) complexes were examined with cryo-electron microscopy and image reconstruction techniques. Native HRV14 virions appear as smooth, rather featureless particles in electron micrographs (Fig. 1*a*). In contrast, bound IgG was readily visible as clumps of electron density closely associated with the outer surfaces of the frozen-hydrated IgG complexes (Fig. 1*b*). The IgG did not cause appreciable particle aggregation under these buffer conditions.

The electron density of the bound IgG appears as an arch-like feature with two arms that attach to the virion near adjacent fivefold axes (Fig. 2*a*) and connect each other above the virion surface at the nearest icosahedral twofold axis. The Fab–virus complex (Fig. 2*b*) is quite similar to the IgG–virus complex with the exception that the Fab arms in the Fab complex are not connected at the twofold axis. In each of these maps, the features of the virion surface closely resemble those of the native HRV14 (Fig. 2*c*). The two reconstructed electron density maps are displayed in Fig. 2 with the same surface contour level, and the connecting electron density in the IgG persists even at contour levels at which portions of the virion electron density disappear. Thus, the bivalent attachment of the IgGs across the twofold axes, as observed in the reconstruction, is a statistically well-defined feature. The Fc region of the antibody was only visible at a contour level that approached the noise level of the reconstruction. This is likely a consequence of the extremely flexible nature of the hinge region (11, 12). The densities of the Fab arms and the capsid are of comparable intensity, thus implying that the 60 NIm-IA sites are nearly saturated with antibody. This result confirms previous studies that demonstrated that mAb17-IA binds with a stoichiometry of 30 per virion and purified IgG–virus complexes do not aggregate even during long incubation times (6, 16).

Although cryo-electron microscopy image reconstruction studies do not yield atomic resolution electron density maps, they have proven to be remarkably accurate. A previously reported Fab–virus complex described the positioning of the Fab molecule to be accurate to within ≈4 Å (17). Recent electron microscopy studies of the bacteriophage ϕX174 accurately described small protrusions, ≈9 Å at the base and ≈23 Å long, that were found at the threefold axes of the atomic structure (18). These results suggest that we should be able to detect distortions in the capsid of the order of ≈10 Å. Therefore, because the virion surface features in Fab and IgG complexes appear to be identical to the native HRV14, bivalent binding apparently does not induce gross conformational changes in the capsid of this magnitude. This further supports the notion that antibody-mediated neutralization is not due to large rearrangements of the capsid structure but probably is due to steric blockage of receptor attachment or stabilization of the capsid by interpentameric cross-linking.

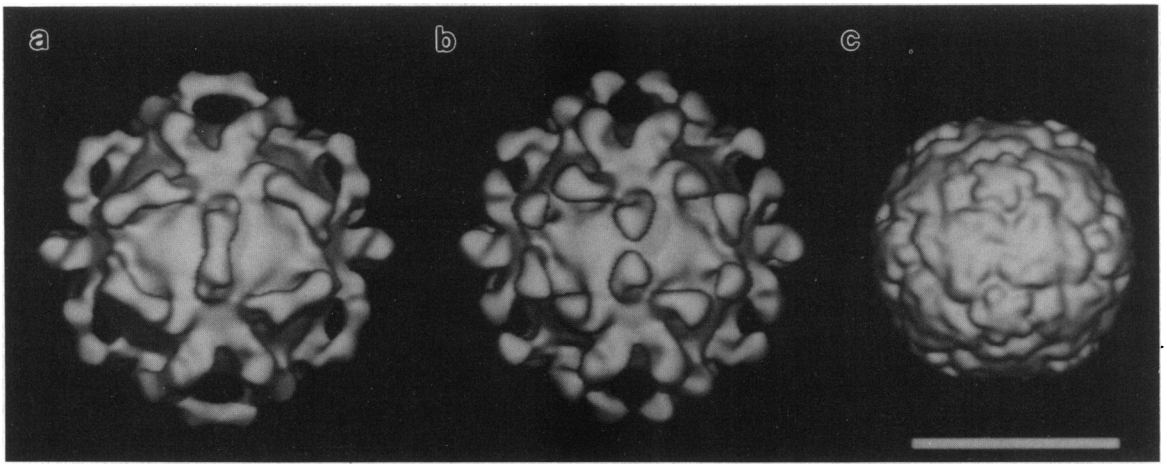

FIG. 2. Three-dimensional reconstructions of the IgG–virus complex (*a*) and of the Fab–virus complex (*b*) and a surface representation of the atomic map of HRV14 (6) truncated to 20-Å resolution (*c*). The surface representations in *a* and *b* were calculated at equivalent contour levels. (Bar = 250 Å.)

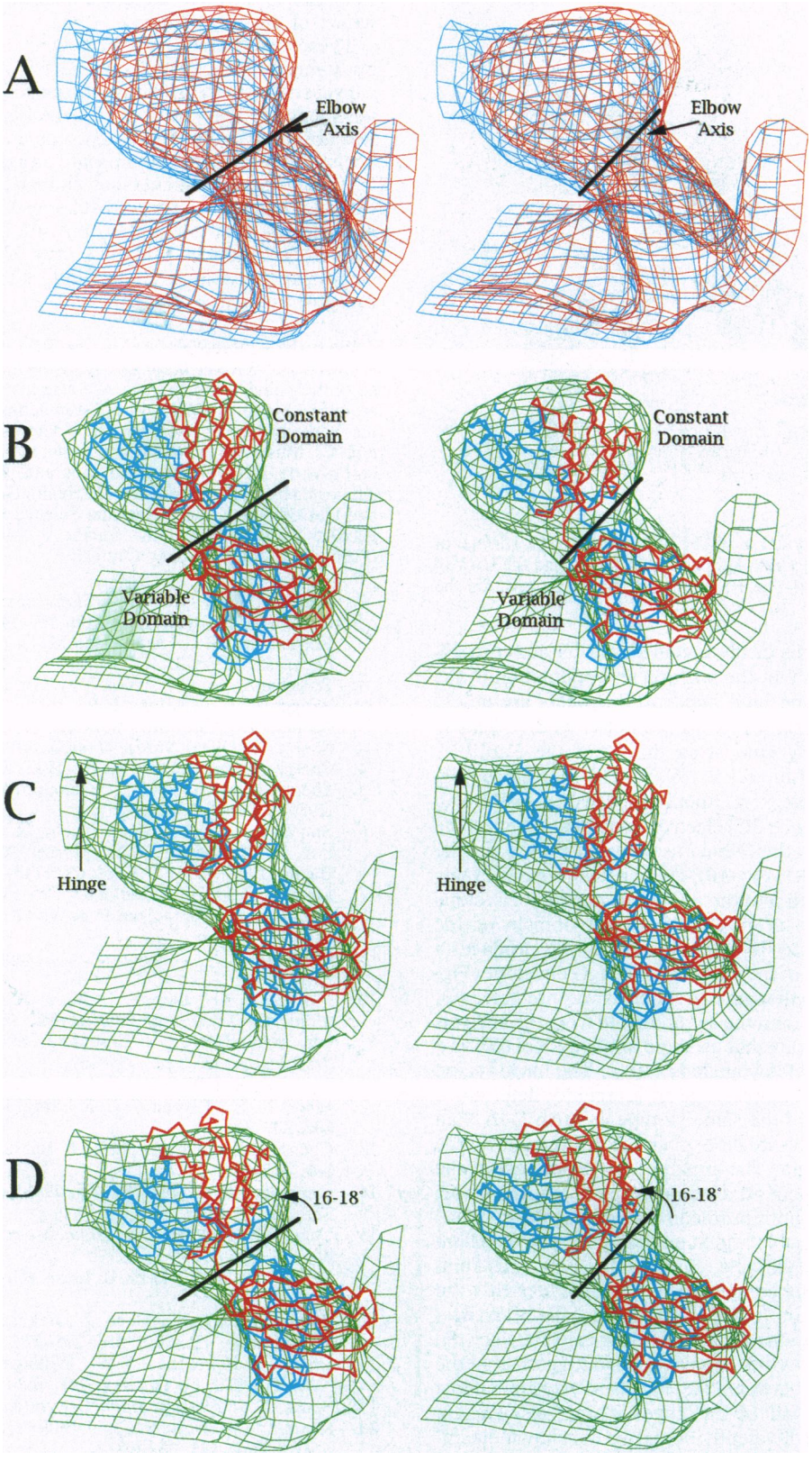

FIG. 3. Stereo diagrams of the Fab and IgG electron density maps. (*A*) Electron density of portions of bound Fab17-IA (red) and mAb17-IA (blue). The nearest icosahedral fivefold axis is on the right side of the diagram, the nearest twofold axis is on the left, and the interior of the particle is towards the bottom of the diagram. (*B*) The atomic model of Fab17-IA fits into the image reconstruction of the Fab–virus complex. Electron density is green, Fab light chain is blue, and Fab heavy chain is red. The orientation is identical to that of *A*. (*C*) The model of Fab17-IA in the same orientation as depicted in *B* displayed with the IgG–virus complex envelope. The view and the color-coding in *C* and *D* are the same as in *B*. (*D*) Model of bound Fab17-IA, with the constant domain orientation and position altered by a rotation of ≈16–18° about the elbow axis, fitted to the IgG–virus complex envelope. The density connecting the two Fab arms at the twofold axis is predominantly due to interactions between the carboxyl termini of the light chains. The remaining unfilled density in this region presumably arises from the hinge peptides that are not included in this atomic model.

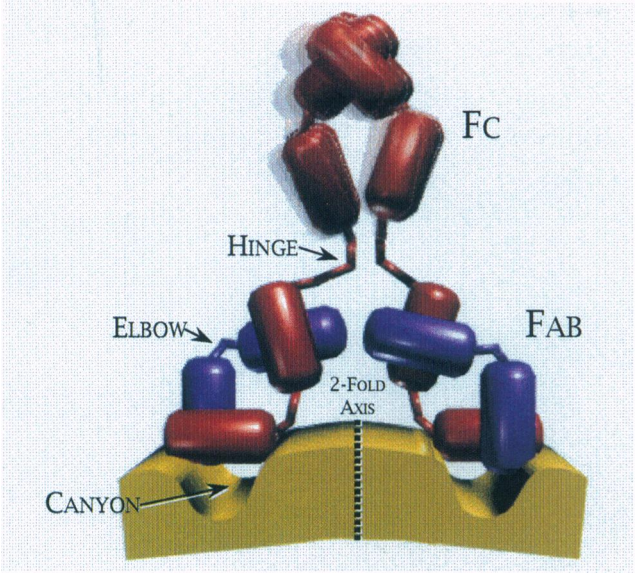

FIG. 4. Schematic model of mAb17-IA bound to the surface of HRV14. Heavy chains are red, light chains are blue, and the HRV14 capsid protein is yellow. The RNA interior would be towards the bottom of the diagram.

Detailed comparisons of the bound Fab17-IA and mAb17-IA molecules showed that the position and orientation of the variable domains of the IgGs and Fab fragments are nearly identical, but the constant regions are not (Fig. 3*A*). This is further exemplified by comparing the fit of the Fab17-IA atomic structure (H. Liu, T.J.S., W. M. Lee, D. Lieppe, A. Mosser, and R. R. Rueckert, unpublished work) in the Fab (Fig. 3*B*) and the IgG (Fig. 3*C*) electron densities. Whereas the envelope of the Fab in the Fab–virus complex closely fits the Fab17-IA atomic model (Fig. 3*B*), the constant regions of this model do not fit as well into the IgG–virus complex envelope (Fig. 3*C*). A rotation of just the constant domain of the Fab17-IA model by ≈16–18° about the elbow axis produces a much better overall fit of the model into the IgG envelope (Fig. 3*D*). This rotation is in the same direction as was predicted (6), but the rotation is less than the 36° predicted from the analysis of the Fab–virus complex that used the antibody Kol (20) as a model. The resulting elbow angle is ≈180°. The hinge region of mAb17-IA more resembles that of a recently determined mouse antibody (21) of the same isotype as mAb17-IA than that of Kol (20), and this might explain the discrepancy in the predicted rotation angle. The apparent movement about the elbow axes upon bivalent attachment suggests that the elbow region may play an important role in maximizing the contacts between the hypervariable region and antigen. The excellent correspondence of the variable regions in the Fab–virus complex and the IgG–virus complex also demonstrates that the variable domains do not "twist" or undergo gross rearrangement upon IgG binding. In addition, this similarity between the IgG–virus and the Fab–virus complexes also suggests that the possible interactions between the Fab heavy chain, elbow region, and the south wall of the canyon (6) may also exist in the IgG complex. The bivalently bound IgG is shown diagramatically in Fig. 4. The two Fab arms of the IgG bind to symmetry-related NIm-IA sites and span an icosahedral two-fold axis. While the antibody does not contact the deeper recesses of the canyon itself, it does occlude access to it. The Fc region is shown as a blurred image to portray the dynamic nature of the hinge region.

These results help to elucidate the mechanisms of antibody-mediated neutralization. Gross rearrangement of the capsid structure as previously proposed (7, 8) is not observed when either Fab17-IA or mAb17-IA binds to HRV14. Just as was observed in the Fab–virus complex (6), the IgG molecule occludes the receptor binding site on HRV14 (3, 14), and this fact supports experiments that showed that mAb17-IA blocks cell attachment (6). These results also support the previous hypothesis that strongly neutralizing antibodies bind bivalently to the capsid and may block disassembly by stabilizing the virions (10) in addition to interfering with cell receptor binding.

We thank R. Rueckert, A. Mosser, W. Lee, and D. Leippe at the University of Wisconsin for supplying the mAb17-IA hybridoma and all of their advice and support. We also thank M. Rossmann for the atomic coordinates of HRV14 and stimulating discussions, H. Liu for his work on the Fab17-IA structure determination and refinement, and C. Music for photography. The programs FRODO (22) and MACINPLOT II (19) were used to create Fig. 3. This work was supported by National Institutes of Health Grants GM10704 to T.J.S. and GM33050 to T.S.B., National Science Foundation Grant MCB 9206305 to T.S.B., and the Lucille P. Markey Charitable Trust (Purdue Structural Biology Center).

1. Rueckert, R. R. (1990) in *Virology*, eds. Fields, B. N. & Knipe, D. M. (Raven, New York), pp. 507–548.
2. Rossmann, M. G. & Johnson, J. E. (1989) *Annu. Rev. Biochem.* **58**, 533–573.
3. Rossmann, M. G., Arnold, E., Erickson, J. W., Frankenberger, E. A., Griffith, J. P., Hecht, H. J., Johnson, J. E., Kamer, G., Luo, M., Mosser, A. G., Rueckert, R. R. & Sherry, B. (1985) *Nature (London)* **317**, 145–153.
4. Sherry, B. & Rueckert, R. R. (1985) *J. Virol.* **53**, 137–143.
5. Sherry, B., Mosser, A. G., Colonno, R. J. & Rueckert, R. R. (1986) *J. Virol.* **57**, 246–257.
6. Smith, T. J., Olson, N. H., Cheng, R. H., Liu, H., Chase, E., Lee, W. M., Leippe, D. M., Mosser, A. G., Rueckert, R. R. & Baker, T. S. (1993) *J. Virol.* **67**, 1148–1158.
7. Mandel, B. (1976) *Virology* **69**, 500–510.
8. Emini, E. A., Ostapchuk, P. & Wimmer, E. (1983) *J. Virol.* **48**, 547–550.
9. Colonno, R. J., Callahan, P. L., Leippe, D. M. & Rueckert, R. R. (1989) *J. Virol.* **63**, 36–42.
10. Mosser, A. G., Leippe, D. M. & Rueckert, R. R. (1989) in *Molecular Aspects of Picornavirus Infection and Detection*, eds. Semler, B. L. & Ehrenfeld, E. (Am. Soc. Microbiol., Washington, DC), pp. 155–167.
11. Roux, K. R. (1984) *Eur. J. Immunol.* **14**, 459–464.
12. Wade, R. H., Taveau, J. C. & Lamy, J. N. (1989) *J. Mol. Biol.* **206**, 349–356.
13. Cheng, R. H., Olson, N. H. & Baker, T. S. (1992) *Virology* **186**, 655–668.
14. Crowther, R. A. (1971) *Philos. Trans. R. Soc. London B* **261**, 221–230.
15. Cheng, R. H. (1992) *Proc. Annu. Meet. Electron Microsc. Soc. Am.* **50**, 996–997.
16. Leippe, D. M. (1991) Ph.D. thesis (Univ. of Wisconsin, Madison).
17. Wang, G., Porta, C., Chen, Z., Baker, T. S. & Johnson, J. E. (1992) *Nature (London)* **355**, 275–278.
18. Olson, N. H., Baker, T. S., Willingmann, P. & Incardona, N. L. (1992) *J. Struct. Biol.* **108**, 168–175.
19. Smith, T. J. (1993) *J. Appl. Crystallogr.*, in press.
20. Marquart, M., Deisenhofer, J., Huber, R. & Palm, W. J. (1980) *J. Mol. Biol.* **141**, 369–391.
21. Harris, L. J., Larson, S., Hasel, K. W., Day, J., Greenwood, A. & McPherson, A. (1992) *Nature (London)* **360**, 369–372.
22. Jones, T. A. (1992) in *Computational Crystallography*, ed. Sayre, D. (Clarendon, Oxford), pp. 303–317.